3. Although salting-in agents, and other denaturants such as urea, are often described as water "structure breakers", our evidence is that they function not by making cavitation in water easier but instead by directly solvating the hydrocarbon species. This overcomes their tendency to make cavitation more difficult, as revealed in surface tension measurements.

4. The special effects seen in water make it an attractive possible solvent for many organic reactions, not just biochemical processes. These effects occur *because* of, not in spite of, the poor solubility of many organic compounds in water.

*I thank my co-workers, named in the references, for their experimental and intellectual contributions. This work has been supported over the years by the National Institutes of Health.*

# Electron Nuclear Double Resonance (ENDOR) of Metalloenzymes

BRIAN M. HOFFMAN

*Department of Chemistry, Northwestern University, Evanston, Illinois 60208*

*Received February 4, 1991 (Revised Manuscript Received May 3, 1991)*

Electron paramagnetic resonance (EPR) techniques have long been a major tool in efforts to determine the structure and function of metalloenzyme active sites.[1] Much of the information EPR provides about the composition, structure, and bonding of a paramagnetic metal center is obtained through the analysis of the hyperfine coupling constants that represent interactions between the spin of the unpaired electron(s) and the spins of nuclei associated with the metal center, endogenous ligands, or bound substrate.[2] These coupling constants are calculated from splittings seen in the EPR spectrum, but for most metallobiomolecules, the splittings are not resolvable and the information they carry is lost. Electron nuclear double resonance (ENDOR) spectroscopy recovers this information.[3]

An ENDOR experiment provides an NMR spectrum of those nuclei that interact with the electron spin of the paramagnetic center, and the ENDOR frequencies directly give the electron-nuclear coupling constants. The occurrence of a nuclear resonance transition is not detected directly, but rather as a change in the EPR signal intensity, hence the classifications as a double-resonance technique. As an NMR method the spectral *resolution* of ENDOR can be as much as 3 orders of magnitude better than that of conventional EPR, and this permits the detection and characterization of electron-nuclear hyperfine interactions for systems whose EPR spectra show no hyperfine splittings. Moreover, ENDOR spectroscopy is inherently *broad-banded*: It is comparably easy to detect ENDOR signals from every type of nucleus. In our studies of biomolecules we have examined signals from $^{1}H$, $^{2}H$, $^{13}C$, $^{14,15}N$, $^{17}O$*, $^{33}S$*, $^{57}Fe$, $^{61}Ni$*, $^{63,65}Cu$*, and $^{95,97}Mo$* nuclei that are present either as constitutive components of a metalloenzyme active site or as part of a bound ligand or substrate, with (*) indicating the first such investigation. This list shows that with proper isotopic labeling it is possible to characterize *every* type of atomic site associated with a paramagnetic center, as we have done in the study of aconitase.[5] With these benefits goes the additional virtue of *selectivity*. Only nuclei that have a hyperfine interaction with the electron-spin system being observed give an ENDOR signal. For example, unlike the case of Mössbauer spectros-

**Table I.**
**Representative Metalloenzyme Active Sites**

| well-characterized | "black boxes" |
|---|---|
| blue copper proteins[10] | nitrogenase[6] |
| heme proteins[9] | Fe-hydrogenase I, II[14] |
| **resting state** | **reaction intermediates** |
| nitrogenase | horseradish peroxidase, Cpd I[11] |
| Ni-hydrogenase (Ni A, B)[13] | cytochrome *c* peroxidase, ES[12] |
| sulfite reductase[15a] | Ni-hydrogenase (Ni C)[13] |
| cytochrome oxidase, $Cu_A$[16a] | sulfite reductase, doubly reduced[15b] |
| | cytochrome oxidase, $Cu_B$[16b] |
| **active-site structure** | **substrate interactions** |
| nitrogenase[6] | aconitase[5a-c] |
| Rieske [2Fe-2S] center[8] | Fe-hydrogenase I, II[14] |
| aconitase[5d] | CO dehydrogenase[17] |
| | xanthine oxidase[18] |

Brian M. Hoffman earned a S.B. degree at The University of Chicago in 1962 and a Ph.D. from Caltech (with Harden McConnell) in 1966. After a postdoctoral year at MIT (with Alex Rich), he joined the faculty at Northwestern University, where he holds a joint appointment in the Department of Chemistry and in the BMBCB Department. In addition to this work in magnetic resonance, members of his group are engaged in studies of long-range electron transfer within protein complexes, as well as in the synthesis and characterization of new molecular metals and magnets. He and his wife boast of four daughters that have a current average age of 11.3 years, with a mean-square deviation of 103 years squared.

(1) (a) For example: Beinert, H.; Griffiths, D. E.; Wharton, D. C.; Sands, R. H. *J. Biol. Chem.* **1962**, *237*, 2337-2346. (b) *Advanced EPR*; Hoff, A. J., Ed.; Elsevier: Amsterdam, 1990.

(2) Atherton, N. M. *Electron Spin Resonance*; Halstead: New York, 1973. Abragram, A.; Bleaney, B. *Electron Paramagnetic Resonance of Transition Ions*; Clarendon Press: Oxford, 1970.

(3) (a) Feher, G. *Phys. Rev.* **1959**, *114*, 1219-1244. (b) Schweiger, A. *Structure and Bonding*; Springer-Verlag: New York, 1982; Vol. 51. (c) Mobius, K.; Lubitz, W. *Biological Magnetic Resonance*; Berliner, L. J., Reuben, J., Eds.; Plenum Press: New York, 1987; Vol. 7, Chapter 3, pp 129-247.

(4) Hoffman, B. M.; Gurbiel, R. J.; Werst, M. M.; Sivaraja, M., in ref 1b, pp 541-591.

(5) (a) Telser, J.; Emptage, M. H.; Merkle, H.; Kennedy, M. C.; Beinert, H.; Hoffman, B. M. *J. Biol. Chem.* **1986**, *261*, 4840-4846. (b) Kennedy, M. C.; Werst, M.; Telser, J.; Emptage, M.; Beinert, M. H.; Hoffman, B. M. *Proc. Natl. Acad. Sci. U.S.A.* **1987**, *84*, 8854-8858. (c) Werst, M. M.; Kennedy, M. C.; Beinert, H.; Hoffman, B. M. *Biochemistry* **1990**, *29*, 10526-10532. (d) Werst, M. M.; Kennedy, M. C.; Houseman, A. L. P.; Beinert, H.; Hoffman, B. M. *Biochemistry* **1990**, *29*, 10533-10539.

0001-4842/91/0124-0164$02.50/0 

copy, it is possible to examine $^{57}Fe$ resonances from one particular metal cluster without interference from other clusters that are present, as is seen best in the case of the nitrogenase MoFe protein.[6] Finally, although measurements typically are performed at low temperatures and employ frozen-solution samples, an ENDOR spectrum generally involves only a subset of molecules with defined, *selected orientations*.[7,4] This allows us not only to deduce bonding characteristics but even to determine active-site geometries, as in the case of the Rieske [2Fe-2S] centers.[8]

The breadth of the technique's applicability perhaps is best discussed by considering representative ENDOR investigations of metalloenzymes in terms of a nonexclusive set of categories (Table I). For example, a site may be "well-characterized", perhaps with a known crystal structure as with the type-1 copper ($Cu^{2+}$) centers, and the goal of a study may be a deeper understanding of its electronic structure and a comparison of family members.[10] In contrast, it might be a "black box" such as the molybdenum–iron cofactor of the nitrogenase MoFe protein.[6] In this case, not even the composition of the center is agreed upon, and ENDOR measurements are of importance even at the level of elemental analysis. Of course, "resting state" systems are the easiest to study, but there are also many cases where it is possible to examine "reaction intermediates". Finally, it is important not only to study the "active-site structure" but also to address the mechanism of enzyme function by probing "substrate interactions".

The remainder of this Account will first describe the ENDOR technique and then use examples to illustrate its power to answer specific questions about important systems. The systems discussed are labeled according to the classification scheme of Table I.

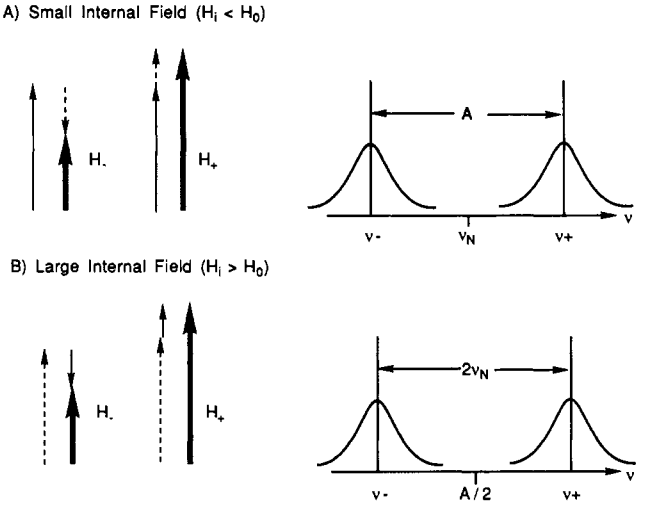


**Figure 1.** Schematic representation of the manner in which external field ($H_0$; →) and internal hyperfine field ($H_i$; - - →) add to give two possible resultant fields with magnitudes $H_\pm$ (⟹) and two-line ENDOR spectra (eq 1). (A) Small internal field as seen for protons. (B) Large internal field, more typical for other nuclei. The resulting ENDOR spectra are schematized to the left.

## The ENDOR Measurement

In an ENDOR experiment a paramagnetic center is placed in a static magnetic field, $\mathbf{H}_o$, and subjected to a radiofrequency field whose frequency is swept as would be done in a continuous wave (CW) NMR experiment; change in the center's EPR signal intensity constitutes the ENDOR response. In a diamagnetic molecule, nucleus N would exhibit a single NMR line centered at its Larmor frequency ($\nu_N$), as determined by the magnitude of the external field, $H_o = |\mathbf{H}_o|$, and its nuclear $g$ factor: $h\nu_N = g_N\beta_n H_o$, where $\beta_n$ is the nuclear magneton, a fundamental constant. However, a hyperfine-coupled nucleus in a paramagnetic center feels a second magnetic field in addition to the external applied field: the hyperfine interaction with the electron spin appears to the nucleus as an "internal" field with magnitude $H_i^N \equiv hA^N/2g_N\beta_n$, where $A^N$ is the hyperfine coupling constant. As shown in Figure 1, where the spin is up the two fields add, and when it is down they subtract (for positive $A^N$). Thus when the electron spin relaxes slowly, the magnitude of the net field experienced by a nucleus has one of two values, $H_\pm^N = |H_o \pm H_i^N|$. Correspondingly, the ENDOR (NMR) response comprises two lines, not one, with the resonance frequencies in first approximation given by[2,4,19]

$$h\nu_\pm^N = g_N\beta_n|H_o \pm H_i^N| = g_N\beta_n H_\pm^N = h\left|\nu_N \pm \frac{A^N}{2}\right| \quad (1)$$

For a proton in a biological system, the external field is larger than the internal field ($\nu_H > A^H/2$) and according to eq 1 the $^1H$ ENDOR spectrum is a hyperfine-split doublet that is centered at the free-proton

(6) (a) True, A. E.; Nelson, M. J.; Venters, R. A.; Orme-Johnson, W. H.; Hoffman, B. M. *J. Am. Chem. Soc.* **1988**, *110*, 1935–1943. (b) Hoffman, B. M.; Roberts, J. E.; Orme-Johnson, W. H. *J. Am. Chem. Soc.* **1982**, *104*, 860–862. (c) McLean, P. A.; True, A. E.; Nelson, M. J.; Chapman, S.; Godfrey, M. R.; Teo, B.-K.; Orme-Johnson, W. H.; Hoffman, B. M. *J. Am. Chem. Soc.* **1987**, *109*, 943–945.

(7) Hoffman, B. M.; Martinsen, J.; Venters, R. A. *J. Magn. Reson.* **1984**, *59*, 110–123. Hoffman, B. M.; Venters, R. A.; Martinsen, J. *J. Magn. Reson.* **1985**, *62*, 537–542. Hoffman, B. M.; Gurbiel, R. J. *J. Magn. Reson.* **1989**, *82*, 309–317.

(8) Gurbiel, R. J.; Batie, C. J.; Sivaraja, M.; True, A. E.; Fee, J. A.; Hoffman, B. M.; Ballou, D. P. *Biochemistry* **1989**, *28*, 4861–4871.

(9) Scholes, C. P. *Multiple Electron Resonance Spectroscopy*; Dorio, M. M., Freed, J. H., Eds.; Plenum Press: New York, 1979; Chapter 8, pp 297–329. Kappl, R., Hütterman, J., in ref 1b, pp 501–540.

(10) Roberts, J. E.; Cline, J. F.; Lum, V.; Gray, H. B.; Freeman, H.; Peisach, J.; Reinhammer, B.; Hoffman, B. M. *J. Am. Chem. Soc.* **1984**, *106*, 5324. Werst, M. M.; Davoust, C. E.; Hoffman, B. M. *J. Am. Chem. Soc.*, in press.

(11) Roberts, J. E.; Hoffman, B. M.; Rutter, R.; Hager, L. P. *J. Biol. Chem. Soc.* **1981**, *256*, 2118–2121. Roberts, J. E.; Hoffman, B. M.; Rutter, R.; Hager, L. P. *J. Am. Chem. Soc.* **1981**, *103*, 7654–7656.

(12) (a) Hoffman, B. M.; Roberts, J. E.; Kang, C. H.; Margoliash, E. *J. Biol. Chem.* **1981**, *256*, 6556. (b) Sivaraja, M.; Goodin, D. B.; Smith, M.; Hoffman, B. M. *Science* **1989**, *245*, 738–740.

(13) Fan, C.; Teixeira, M.; Moura, J.; Moura, I.; Huynh, B.-H.; Le Gall, J.; Peck, H. D., Jr.; Hoffman, B. M. *J. Am. Chem. Soc.* **1991**, *113*, 20–25.

(14) Telser, J.; Benecky, M. J.; Adams, M. W. W.; Mortenson, L. E.; Hoffman, B. M. *J. Biol. Chem.* **1987**, *262*, 6589–6594.

(15) (a) Stevens, T. H.; Martin, C. T.; Wang, H.; Brudvig, G. W.; Scholes, C. P.; Chan, S. I. *J. Biol. Chem.* **1982**, *259*, 112–123. Hoffman, B. M.; Roberts, J. E.; Swanson, M.; Speck, S. H.; Margoliash, E. *Proc. Natl. Acad. Sci. U.S.A.* **1980**, *77*, 1452–1456. (b) Cline, J.; Reinhammer, B.; Jensen, P.; Venters, R.; Hoffman, B. M. *J. Biol. Chem.* **1983**, *258*, 5124–5128.

(16) (a) Cline, J. F.; Janick, P. A.; Siegel, L. M.; Hoffman, B. M. *Biochemistry* **1985**, *24*, 7942–7947. (b) Cline, J. F.; Janick, P. A.; Siegel, L. M.; Hoffman, B. M. *Biochemistry* **1986**, *25*, 4647–4654.

(17) Fan, C.; Gorst, C. M.; Ragsdale, S. W.; Hoffman, B. M. *Biochemistry*, in press.

(18) Howes, B. D.; Pinhal, N. M.; Turner, N. A.; Bray, R. C.; Anger, G.; Ehrenberg, A.; Raynor, J. B.; Lowe, D. J. *Biochemistry* **1990**, *29*, 6120–6127.

(19) For completeness we note that a nucleus with $I > 1/2$ will possess a quadrupole moment that interacts with the total charge distribution of its surroundings. This interaction, if resolved, splits each of the two lines at $\nu_\pm^N$ (eq 1) into $2I$ lines, with transitions at frequencies given (approximately) by the following (ref 2 and 4): $\nu_\pm(m) = |A^N/2 \pm \nu_N + (3P^N/2)(2m - 1)|$, where $P^N$ is the quadrupole coupling constant. The quadrupole coupling gives important information about bonding in the metal center and is not observable in ordinary EPR spectra even when hyperfine splittings are observed.

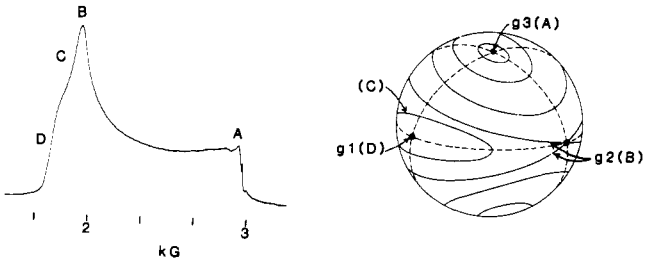


**Figure 2.** Correspondences between magnetic field values in an EPR spectrum and field orientations within the molecular $g$ frame. Left: X-band EPR absorption envelope for a center with a rhombic **g** tensor, $g_1 > g_2 > g_3$. Right: Unit sphere with orientation subsets of constant $g$ factor indicated, each corresponding to a single observing field; several correspondences are indicated. Reprinted with permission from ref 6a. Copyright 1988 American Chemical Society.

Larmor frequency $\nu_H$ (42.6 MHz at $H_o$ = 10 kG) and split by $A^H$: $\nu_\pm{}^H = \nu_H \pm A^H/2$ (Figure 1A). For a given $g$ value of observation, $\nu_H$ is proportional to the microwave frequency of the ENDOR spectrometer, $\nu(m)$; the center of the $^1$H ENDOR pattern shifts correspondingly (eq 1). For example, in a conventional X-band spectrometer, $\nu(m) \sim 9$ GHz and the $^1$H resonances are centered at $N_H \sim 14$ MHz, whereas in our Q-band spectrometer, $\nu(m) \sim 35$ GHz and $\nu_H \sim 52$ MHz.

In contrast, for nonprotonic nuclei, the internal field typically is the larger ($A^N/2 > \nu_N$) and the ENDOR pattern is a Larmor-split doublet centered at $A^N/2$ and split by $2\nu_N$: $\nu_\pm{}^N = A^N/2 \pm \nu_N$ (Figure 1B). Because the center of such a pattern is determined by a molecular parameter, $A^N/2$, it does not shift with the spectrometer microwave frequency. This difference between the ENDOR behavior of protons and other nuclei is very useful. In most of the systems listed in Table I, $^1$H signals in an X-band spectrometer overlap with and obscure signals from other nuclei (e.g., $^{14}$N, $^{57}$Fe, $^{17}$O, ...) that appear in the range of 0–30 MHz. This problem is eliminated by shifting the proton pattern to high frequency in a Q-band spectrometer (e.g., ref 10).

The samples employed in ENDOR studies of metalloenzymes almost always are frozen solutions. This means that the EPR envelope is a superposition of signals associated with a random distribution of all possible orientations (Euler angles $\theta$ and $\phi$) of the applied magnetic field, $\mathbf{H}_o$, with respect to the molecular framework. However, we recognized that when a molecule exhibits resolved anisotropic magnetic interations, namely, anisotropic **g**, hyperfine, and/or zero-field splitting tensors, then at each value of the applied field, the EPR intensity, and thus the ENDOR response, arises only from a corresponding, restricted subset of these orientations. This is not only true at the high- and/or low-field edges of the EPR envelope, which actually represent single-crystal-like situations where the field happens to be along a **g**-tensor axis:[20] at each intermediate field the response is from a restricted and mathematically well developed subset of orientations[7] (Figure 2).

A series of ENDOR spectra collected at fields ($g$ values) across the EPR envelope of a polycrystalline sample thus explores different subsets of molecular orientations in a clear analogy to the way that a series of spectra collected while a single crystal is rotated explores different individual orientations. This correspondence of field and orientations (angle selection) serves as the basis of the analysis procedure we have developed[4,6-8] for obtaining complete hyperfine tensors—both the principal values *and* the orientation of the tensor relative to the molecular framework—from ENDOR studies of polycrystalline (frozen-solution) samples. The procedure has been applied to the majority of the cases listed in Table I and is illustrated below.

(20) Rist, G. H.; Hyde, J. S. *J. Chem. Phys.* **1970**, *52*, 4633–4643.

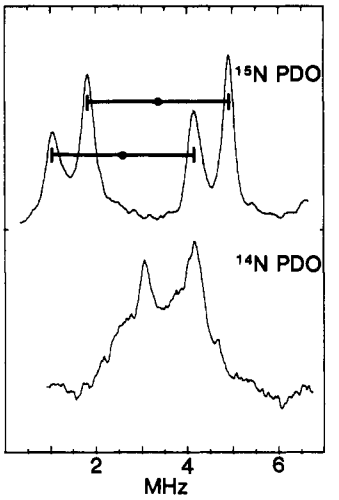


**Figure 3.** ENDOR spectra of $^{15}$N-enriched and $^{14}$N natural abundance PDO from *P. cepacia* taken at $g_2$ = 1.92. The assignments to $A/2$ (•) and $2\nu_N$ (|—|) of each doublet are indicated. Conditions: $H_o$ = 0.3596 ($^{14}$N), 0.3588 T ($^{15}$N): $T$ = 2 K. Reprinted with permission from ref 8. Copyright 1989 American Chemical Society.

## Active-Site Structure: Rieske [2Fe-2S] Center of Phthalate Dioxygenase

Studies during the quarter of a century since the Rieske center's discovery[21] established the presence of an unusual [2Fe-2S] cluster but failed to establish the structural differences distinguishing it from the ferredoxin-type [2Fe-2S] clusters that are coordinated to proteins by four cysteine ligands.[22] To resolve this question, in collaboration with Dr. J. A. Fee and Prof. D. Ballou we performed 9- and 35-GHz ENDOR studies on the Rieske-type center of globally and selectively $^{15}$N enriched phthalate dioxygenase (PDO) prepared from *Pseudomonas cepacia*.[8]

**Ligand Identification.** Four different samples of *P. cepacia* phthalate dioxygenase were prepared, each with a specific labeling pattern. The X-band ENDOR spectrum at $g_2$ of natural-abundance PDO (sample 1) shows a broad pattern of $^{14}$N resonances that by itself is not amenable to analysis (Figure 3). In contrast, spectra of globally $^{15}$N enriched PDO (sample 2) taken at $g_2$ exhibit two sharp Larmor-split doublets from $^{15}$N that are centered at $A(^{15}N)/2$ = 2.55 and 3.35 MHz and that show the expected splitting of $2\nu(^{15}N)$ = 3.1 MHz (eq 1). Assignment of these doublets to two magnetically distinct $^{15}$N-labeled nitrogenous ligands coordi-

(21) Rieske, J. S.; Machennan, D. H.; Coleman, R. *Biochem. Biophys. Res. Commun.* **1964**, *15*, 338–344. Rieske, J. S.; Zaugg, W. S.; Hansen, R. E. *J. Biol. Chem.* **1964**, *239*, 3023–3030.

(22) See: Fee, J. A.; Kuila, D.; Mather, M. W.; Yoshida, T. *Biochim. Biophys. Acta* **1986**, *853*, 153–185.

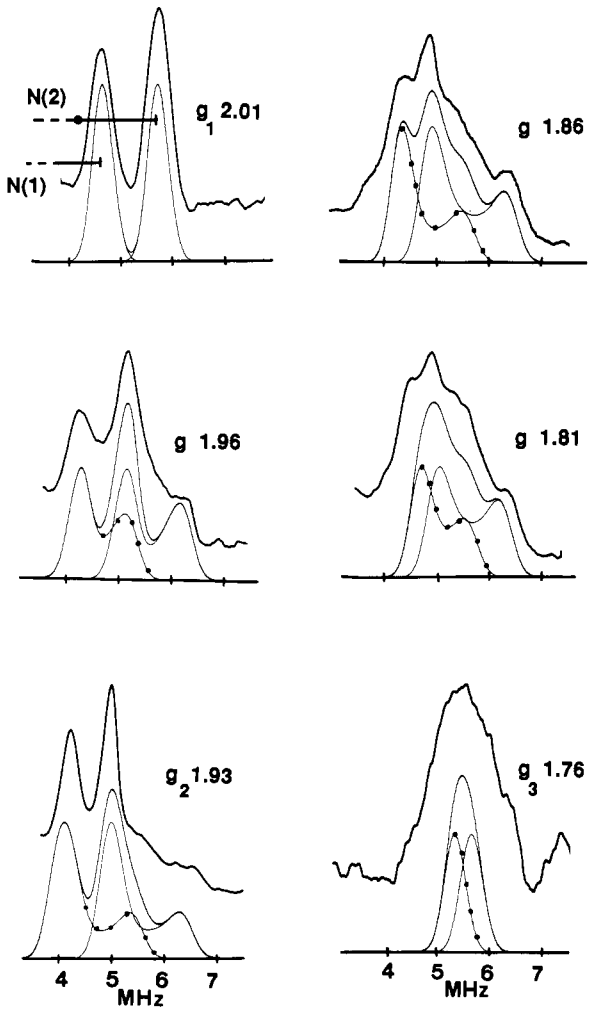


**Figure 4.** ENDOR spectra of the two $^{15}N$ bound to the cluster of PDO, showing the $\nu_+$ resonances (eq 1) at selected magnetic fields. Computer simulations for $^{15}N(1)$ and $^{15}N(2)$ employ the hyperfine interaction parameters given in ref 8 and are shown below the corresponding spectra; the bold line is the sum of the simulations. The component line widths were taken to be equal for the two sites (0.2 MHz) and independent of angle; relative intensities for the individual sites are normalized; spectra were simulated with EPR line widths of 2.0 mT. Conditions: $T = 2$ K, with a microwave frequency of 9.6 GHz and $g$ values as indicated. Reprinted with permission from ref 8. Copyright 1989 American Chemical Society.

nated to the [2Fe-2S] cluster is confirmed by single-crystal-like spectra taken at $g_1$. These two ligands are further identified as histidines by ENDOR measurements on PDO *specifically* labeled with [$^{15}N$]histidine.

**Determination of $^{15}N$ Hyperfine and $^{14}N$ Quadrupole Tensors.** $^{15}N$ X-band ENDOR spectra of enriched PDO were measured across the EPR envelope, and the $^{15}N$ hyperfine tensors for the two coordinated histidyl nitrogens were determined by using the analysis procedures mentioned above. As seen in the selected $^{15}N$ spectra presented in Figure 4, simulations using the two hyperfine tensors reported in ref 8 fully reproduce not only the positions of the two sharp resonances but also the breadth of the pattern to higher frequency and other resolved features. The reported tensors were determined by simulating spectra at all observing fields, and the full set of data shows the same good agreement.

Interestingly, the two hyperfine tensors, and thus the two Fe–N bonds, are quite inequivalent, with largest tensor components of $A_3(N1) = 8.1$ MHz and $A_3(N2)$ = 9.8 MHz. The combination of data from ENDOR, Mössbauer, and Raman spectroscopies indicates that both histidines are coordinated to the $Fe^{2+}$ site of the reduced cluster, and thus the inequivalence does *not* stem from binding to Fe ions of different valency. The quadrupole tensors[19] for the two $^{14}N$ ligands also were determined, a novel approach being used to analyze the field dependence of the $^{14}N$ signals.

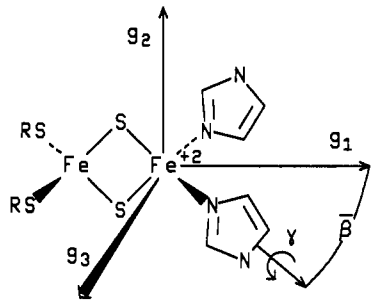


**Figure 5.** Structure of the Rieske-type [2Fe-2S] cluster of PDO as determined by ENDOR spectroscopy. The [2Fe-2S] core and the $(g_1g_2)$ plane lie in the paper; the bite angles, $\bar{\beta}$, and dihedral angles, $\gamma$, are discussed in the text. Reprinted with permission from ref 8. Copyright 1989 American Chemical Society.

**Structure of the Cluster.** The hyperfine and quadrupole coupling tensors can be used to derive detailed information about the orbitals involved in the Fe–histidine bond;[2,8] they also give direct geometric information about the cluster. The analysis of the $^{14}N$ hyperfine tensors led to a geometric model (Figure 5) in which the four protein-donated ligands and two iron ions lie in the $g_1g_3$ plane with the Fe–Fe vector corresponding to $g_1$; it gave $\bar{\beta}(N1) \sim 35°$ and $\bar{\beta}(N2) \sim 55°$ for the angles between Fe–N and Fe–Fe vectors. The N–Fe–N bite angle, $\bar{\beta}(1) + \bar{\beta}(2) \sim 90$ (10)°, is consistent with roughly tetrahedral coordination at $Fe^{2+}$, with the inequality $\bar{\beta}_1 \neq \bar{\beta}_2$ again indicating an unsymmetrical structure for the cluster. The analysis of the $^{14}N$ quadrupole tensors further set limits on the dihedral twist of the two imidazole rings out of the N–Fe–N plane ($\gamma$, Figure 5), suggesting that $|\gamma(N1)| \leq 10°$ and that $|\gamma(N2)| > |\gamma(N1)|$. Finally, because the $^{14}N$ and $^{1}H$ ENDOR patterns for the *Thermus* and mitochondrial Rieske proteins are virtually indistinguishable from those of PDO, we inferred that the structure presented here is generally applicable to Rieske-type centers.

## Reaction Intermediate: Cytochrome *c* Peroxidase Compound ES

Cytochrome *c* peroxidase (CcP) catalyzes the $H_2O_2$-dependent oxidation of ferrocytochrome *c* and is capable of storing two oxidizing equivalents following treatment with peroxide.[23,24] In the fully oxidized reactive intermediate, called ES, one of the oxidizing equivalents is stored as the oxy-ferryl ($Fe^{IV}$=O) state of the heme iron with $S = 1$. The second exists as a reversibly oxidized amino acid residue (R•) whose EPR signal is described by an axial **g** tensor without parallel among organic radicals composed of first-row elements: $g_\parallel = 2.04$ and $g_\perp = 2.01$.[12,25,26]

(23) (a) Yonetani, T. *Adv. Enzymol.* **1970**, *33*, 309. Coulson, A. F. W.; Erman, J. E.; Yonetani, T. *J. Biol. Chem.* **1971**, *246*, 917. (b) Hori, H.; Yonetani, T. *J. Biol. Chem.* **1985**, *260*, 349.

(24) Dawson, J. H. *Science* **1988**, *240*, 433. Dawson, J. H.; Sono, M. *Chem. Rev.* **1987**, *87*, 1255.

(25) Wittenberg, B. A.; Kampa, L.; Wittenberg, J. B.; Blumberg, W. E.; Peisach, J. *J. Biol. Chem.* **1968**, *243*, 1863.

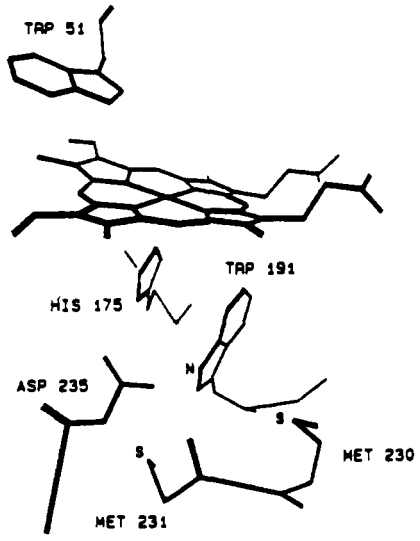


**Figure 6.** Heme environment for CcP showing groups of interest except for Met[172], which is in contact with the heme to the left (courtesy, T. Poulos).

The identity of R• has been sought for almost a quarter of a century, with several species having been proposed. One is a Trp radical[23b] formed from Trp[51] or Trp[191], both of which are in contact with the heme (Figure 6). However, paramagnetic resonance[12a,26] and other[27] data appeared to be inconsistent with this assignment. As an alternative, we proposed that the EPR signal is associated with a nucleophilically stabilized Met radical; Met[172] and a pair of Met residues, 230 and 231, have been considered.[28] To determine the identity of the radical site unambiguously, we collaborated with Prof. D. Goodin in the use of ENDOR spectroscopy to study enzyme selectively deuterated at Trp or Met, as well as samples subjected to H/D solvent exchange.[12b] This nonperturbative approach was augmented by the use of site-directed nutagenesis,[29-31] with the examination of the Trp[51] → Phe mutant.

A proton ENDOR spectrum obtained with ES from the natural-abundance enzyme, sample I (Figure 7A), exhibits a pattern centered at $\nu_H$, characteristic of $H_o > H_i$ (eq 1), with numerous hyperfine-split doublets, eq 1. The hyperfine splittings range from $A^H \sim 20$ MHz to $A^H \sim 3$ MHz; in addition, there is a "distant-ENDOR" peak at $\nu_H$. The $^1$H ENDOR spectrum of ES that contains methionine-$CD_3$, sample II, is identical with that of I (data not shown), immediately forcing the conclusion that the proton resonances of the radical are not associated with *any* of the six Met residues of the protein.

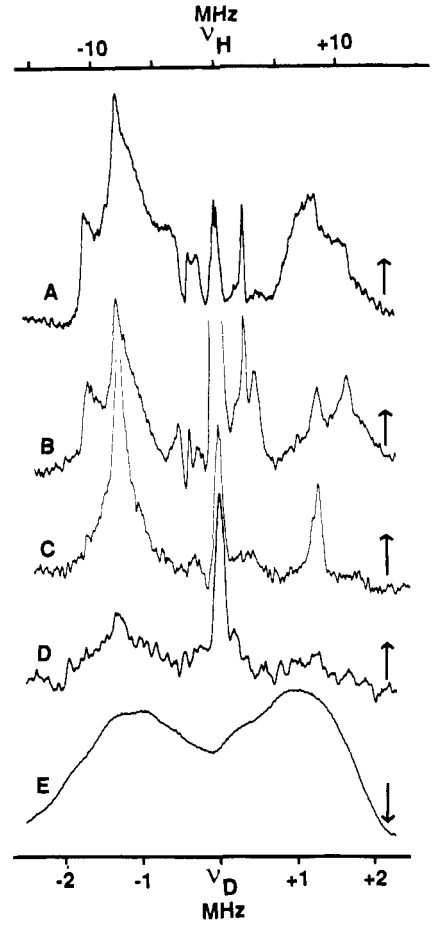


**Figure 7.** Q-band $^1$H and $^2$H ENDOR spectra at $g_\perp = 2.01$ of the ES compound of CcP. Proton spectra: (A) sample I; (B) sample III; (C) sample IV; (C) sample V. Deuteron spectrum: (E) sample V. The proton spectra are presented as $\delta\nu_H = \nu - \nu_H$ (top scale); the proton Larmor frequency is $\nu_H = 53.2$–$53.4$ MHz, depending on the spectrum. The deuteron ENDOR is presented as $\delta\nu_D = \nu - \nu_D$ (bottom scale); the deuteron Larmor frequency is $\nu_D = 7.7$ MHz. Nuclear hyperfine coupling constants for H and D are related by $A^H/A^D = g^H/g^D = 6.514$, and the scales have been adjusted by this factor. Thus a given coupling would cause the same splitting on the H and D spectra, and features in the H and D spectra can be compared directly. Conditions: $T = 2$ K; microwave frequency = 35.3 GHz. Reprinted with permission from ref 12b. Copyright 1989 American Association for the Advancement of Science.

The $^1$H ENDOR spectrum of the residue 51 Trp → Phe mutant (sample III; Figure 7B) also is similar to that of the wild-type sample, Figure 7A, ruling out Trp[51]. Nevertheless, the spectra of parts C and D of Figure 7 definitively identify the radical site as a Trp residue. Deuteration of the Trp constitutive proton, sample IV, suppresses all proton signals from ES with the exception of the distant-ENDOR signal at $\nu_H$ and the intense doublet with $A^H \sim 15$ MHz (Figure 7C). This latter doublet is eliminated when enzyme sample IV is subjected to H/D exchange to produce V (Figure 7D). As the final proof that R• is associated with Trp, the loss of proton resonances upon deuteration of the Trp constitutive protons and of the exchangeable proton in sample V is accompanied by the appearance of the corresponding deuteron ENDOR signal centered at $\nu_D \sim 7.8$ MHz (Figure 7E). Note that the deuteron signals would have been centered at $\nu_D < 2$ MHz in an

(26) Sahlin, M.; Graslund, A.; Ehrenberg, A.; Sjoberg, B.-M. *J. Biol. Chem.* **1982**, *257*, 366–369. Bender, C. J.; Sahlin, M.; Babcock, G. T.; Chandrashekar, T. K.; Salowe, S. P.; Stubbe, J.; Lindstrom, B.; Petersson, L.; Ehrenberg, A.; Sjoberg, B.-M. *J. Am. Chem. Soc.* **1989**, *111*, 8076–8083. Kartheum, R.; Dietz, R.; Nastainczyk, W.; Ruf, H. H. *Eur. J. Biochem.* **1988**, *171*, 313. Klmacy, R. J.; Tsai, A.-L. *J. Biol. Chem.* **1987**, *262*, 10524. Debus, R. J.; Barry, B. A.; Babcock, G. T.; McIntosh, L. *Proc. Natl. Acad. Sci. U.S.A.* **1988**, *85*, 427.

(27) Myers, D.; Palmer, G. *J. Biol. Chem.* **1985**, *260*, 3887.

(28) Edwards, S. L.; Xuong, N. H.; Hamlin, R. C.; Kraut, J. *Biochemistry* **1987**, *26*, 1503.

(29) (a) Goodin, D. B.; Mauk, A. G.; Smith, M. *Proc. Natl. Acad. Sci. U.S.A.* **1986**, *83*, 1295. (b) Goodin, D. B.; Mauk, A. G.; Smith, M. *J. Biol. Chem.* **1987**, *262*, 7719.

(30) (a) Fishel, L. A.; Villafranca, J. E.; Mauro, J. M.; Kraut, J. *Biochemistry* **1987**, *26*, 351. (b) Mauro, J. M.; Fishel, L. A.; Hazzard, J. T.; Meyer, T. E.; Tollin, G.; Cusanovich, M. A.; Kraut, J. *Biochemistry* **1988**, *27*, 6243. (c) Scholes, C. P.; Liu, Y.; Fishel, L. A.; Farnum, M. F.; Mauro, J. M.; Kraut, J. *Isr. J. Chem.* **1989**, *29*, 85–92.

(31) Beinert, H. *Eur. J. Biochem.* **1988**, *186*, 5–15.

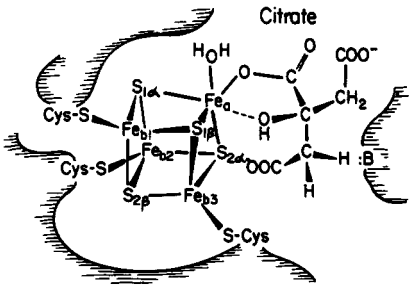


**Figure 8.** Representation of ENDOR-derived information about the [4Fe-4S]$^+$ cluster of the aconitase enzyme–substrate complex, showing the two pairs of sulfur detected by ENDOR, S1$\alpha$,S1$\beta$ and S2$\alpha$,S2$\beta$, in relationship to the four inequivalent iron sites $Fe_a$, $Fe_{b1}$, $Fe_{b2}$ and $Fe_{b3}$, along with the bound substrate. Reprinted with permission from ref 5d. Copyright 1990 American Chemical Society.

X-band spectrometer and likely would have been too weak to characterize.

The results in Figure 7 clearly prove that the paramagnetic species associated with the ($g_{\parallel}$ = 2.04) EPR signal of CcP compound ES is a Trp radical. Of the seven Trp residues in CcP, Trp$^5$ and Trp$^{191}$ are by far nearest to the heme active site (Figure 6) and are implicated by several arguments.[12b] Because the Trp$^{51}$ → Phe mutation causes only minor perturbations in the proton ENDOR pattern, the radical site can only be Trp$^{191}$, not Trp$^{51}$.

## Substrate Interactions and Enzyme Mechanism: Aconitase

Our studies of the enzyme aconitase [citrate (isocitrate) hydro-lyase, EC 4.2.1.3] in collaboration with Prof. H. Beinert and Dr. M. C. Kennedy[5] show how ENDOR spectroscopy can go beyond the determination of active-site composition and electronic and geometric structure: under favorable conditions ENDOR study of substrate interactions can make decisive contributions to the determination of an enzyme mechanism.[31,32] Aconitase catalyzes the stereospecific interconversion of citrate and isocitrate via the dehydrated intermediate *cis*-aconitate. The active site contains a diamagnetic

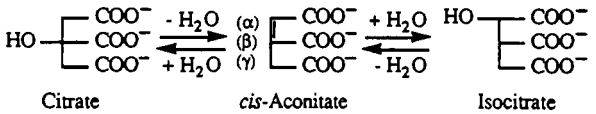


[4Fe-4S]$^{2+}$ cluster that can be reduced to the EPR-active [4Fe-4S]$^+$ state with retention of activity. Surprisingly the cluster does not act in electron transport but rather performs its catalytic function through interaction with substrate at a specific iron site of the cluster ($Fe_a$).[33]

**Cluster Properties.** The $^{57}$Fe ENDOR data clearly confirms the Mössbauer result[33] showing that $Fe_a$ differs from the other three, $Fe_b$, sites of the [4Fe-4S]$^+$ cluster. The data further shows that the $Fe_b$ are themselves inequivalent and that this is true both in the substrate-free enzyme and the enzyme–substrate complex. Analysis of $^{33}$S resonances from the [4Fe-4S]$^+$ cluster of the enzyme–substrate complex suggests that the sulfur sites occur as two pairs ($S_{\alpha 1}$, $S_{\alpha 2}$; $S_{\beta 1}$, $S_{\beta 2}$) with

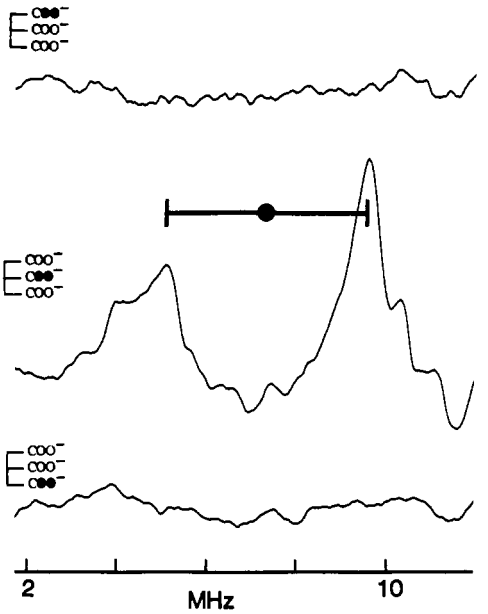


**Figure 9.** $^{17}$O ENDOR spectra at $g$ = 1.85 of reduced aconitase in the presence of substrate whose COO$^-$ groups have been individually labeled with $^{17}$O. Upper: Label at $\alpha$-carboxyl. Middle: Label at $\beta$-carboxyl. Lower: Label at $\gamma$-carboxyl. (•) indicates $A^0/2$, and (|—|) indicates $2\nu_o$. The hydroxyl is not shown in the cartoon substrate because aconitase converts it to an equilibrium mixture (see drawing within text). Conditions: $T$ = 2 K; $H_o$ = 0.3815 T. From ref 5b.

remarkably small spin density on sulfur, and it even discloses their spatial relation to the Fe sites.[5d] Figure 8 summarizes this information about the four Fe and four inorganic sulfides within the context of the X-ray diffraction structure of Robbins and Stout,[34a] which shows that cysteines are bound to the three iron ions that correspond to the three $Fe_b$ seen spectroscopically.

**Structure of the Enzyme–Substrate Complex.** The first question raised by the possible catalytic role of the cluster in a dehydration/hydration reaction is whether solvent $H_xO$ ($H_2O$ or $OH^-$) and/or the OH of substrate can bind to it. Through the use of $^{17}$O, $^1$H, and $^2$H ENDOR we were able to show that the fourth ligand of $Fe_a$ in substrate-free enzyme is a hydroxyl ion from the solvent, and that binding of substrate or substrate analogues to $Fe_a$ causes the hydroxyl species to become protonated to form a bound water molecule. Note that this represents the first demonstration of an exogenous ligand to an iron–sulfur cluster. The studies further suggested that the cluster might simultaneously coordinate the OH of substrate and $H_2O$ of the solvent (Figure 8).

The remaining question is whether one or more carboxyls of substrate bind to the cluster. Figure 9 presents ENDOR spectra of [4Fe-4S]$^+$ aconitase in the presence of citrate whose carboxyl groups have been individually labeled with $^{17}$O. The ENDOR measurements with substrate whose central ($\beta$) carboxyl group is $^{17}$O labeled show a strong $^{17}$O pattern (Figure 9, middle), but no $^{17}$O ENDOR signal was observed when either of the terminal carboxyl groups ($\alpha$ or $\gamma$) was $^{17}$O labeled (Figure 9, upper and lower). Thus, under our experimental conditions the central carboxyl group binds to $Fe_a$, but the two terminal groups ($\alpha$ and $\gamma$) do

(32) Emptage, M. H. In *Metal Clusters in Proteins*; Que, L., Ed.; ACS Symposium Series 372; American Chemical Society: Washington, DC, 1987; pp 343–371.

(33) Kent, T. A.; Emptage, M. H.; Merkle, H.; Kennedy, M. C.; Beinert, H.; Münck, E. *J. Biol. Chem.* **1985**, *260*, 6371–6881.

(34) (a) Robbins, A. H.; Stout, C. D. *Proc. Natl. Acad. Sci. U.S.A.* **1989**, *86*, 3639–3643. (b) Robbins, A. H.; Stout, C. D. *Proteins: Struct., Funct., Genet.* **1989**, *5*, 289–312.

not bind to the cluster. However, the enzyme also is *able* to accommodate substrate bound by the α-carboxyl, as is shown by $^{17}O$ ENDOR of enzyme that has bound a $^{17}O$-enriched isocitrate analogue that lacks the β-carboxyl. Presumably the addition of the negatively charged carboxyl causes protonation of the $OH^-$ that binds to the cluster in the absence of substrate.

The resulting ENDOR-derived structure for the substrate-bound cluster (Figure 8) is remarkably well corroborated by recent X-ray diffraction information.[34b] As seen by ENDOR spectroscopy, the cluster appears to function as follows: (i) it helps to position the substrate through the binding of one carboxyl; (ii) it coordinates and accepts the hydroxyl of substrate during the dehydration of citrate and isocitrate; (iii) it donates a bound hydroxyl during the rehydration of *cis*-aconitate. Further, to accommodate the stereochemistry of the reaction, *cis*-aconitate must disengage from the active site, rotate 180°, and switch the carboxyl that binds before completing the catalytic cycle.

## Conclusion

The few examples presented above have been selected from among many (Table I) to illustrate how the ENDOR technique can answer questions about metalloenzyme structure and function that have resisted other means of approach. An implicit aspect has been the importance of precise isotope labeling as well as our development of procedures for the analysis of frozen-solution ENDOR spectra and of multifrequency capabilities. Work in progress[35] shows that there are further benefits to the utilization of pulsed-ENDOR techniques[36] in addition to CW ENDOR. In short, it is easy to envision continued expansion of the role played by ENDOR spectroscopy in the study of metallobiomolecules.

*In addition to collaborators mentioned above, others associated with projects that could not be mentioned are equally acknowledged, as are the graduate students and postdoctorals whose work is described here. These studies could not have been performed without the technical expertise of Mr. Clark E. Davoust or the support of the NIH, NSF, and USDA.*

(35) Doan, P.; Fan, C.; Davoust, C. E.; Hoffman, B. M. *J. Magn. Reson.*, submitted.
(36) *Modern Pulsed and Continuous Wave Electron Spin Resonance*; Kevan, L., Bowman, M. K., Eds.; Wiley: New York, 1990.

# Scanning Tunneling Microscopy Studies of Low-Dimensional Materials: Probing the Effects of Chemical Substitution at the Atomic Level

CHARLES M. LIEBER* and XIAN LIANG WU

*Department of Chemistry, Columbia University, New York, New York 10027*

*Received January 23, 1991 (Revised Manuscript Received April 15, 1991)*

A major goal of current research efforts in solid-state chemistry and physics is to understand the factors that determine the electronic and structural properties and phase transitions in materials.[1,2] This understanding is essential to the materials sciences since it will lead the way to the rational design and preparation of new solids with predictable properties. A general experimental approach that has been used to probe these factors involves studies of chemically substituted or doped materials.[3-6] Substitutional doping is a useful technique since it can affect systematic variations in the carrier density of a material and, for example, convert a semiconductor to a metal or tune the properties of a metal so that it will become a superconductor. Substitutional doping will also cause disorder in the lattice which can lead to a metal–insulator transition.[6] It is important for new materials design to predict which of these manifestations of doping will dominate.

In the past, the electronic effects of substitutional doping have been investigated by photoelectron and optical spectroscopies and transport measurements, while structural manifestations of doping have been probed by X-ray, neutron, and electron diffraction

Charles M. Lieber received a B.A. with honors in chemistry from Franklin and Marshall College in 1981. He received a Ph.D. from Stanford University in 1985, working with Nathan Lewis on kinetic and catalytic studies of modified electrodes, and then moved to Caltech to pursue postdoctoral research on long-range electron transfer in metalloproteins with Harry Gray. In 1987 he joined the faculty of Columbia University, and he was promoted to Associate Professor of Chemistry in 1990. His current research interests include the chemical physics of solids and interfaces, especially high-temperature superconductivity, charge density waves, and the atomic origins of friction.

Xian Liang Wu received a B.S. from Peking University in 1982 and an M.S. from Hebei University in 1985. He is currently completing a Ph.D. on scanning tunneling microscopy studies of low-dimensional materials with Charles Lieber.

(1) DiSalvo, F. J. *Science* **1990**, *247*, 649.
(2) (a) *Physics Through the 1990s: Condensed-Matter Physics*; National Academy Press: Washington, 1986. (b) *Physics Through the 1990s: Scientific Interfaces and Technological Applications*; National Academy Press: Washington, 1986.
(3) Miller, J. S.; Epstein, A. J. *Angew. Chem., Int. Ed. Engl.* **1987**, *26*, 287.
(4) (a) Rao, C. N. R.; Raveau, B. *Acc. Chem. Res.* **1989**, *22*, 106. (b) Sleight, A. W. *Science (Washington)* **1988**, *242*, 1519. (c) Williams, J. M.; Beno, M. A.; Carlson, K. D.; Geiser, U.; Kao, H. C. I.; Kini, A. M.; Porter, L. C.; Shultz, A. J.; Thorn, R. J.; Wang, H. H. *Acc. Chem. Res.* **1988**, *21*, 1.
(5) (a) Dresselhaus, M. S.; Dresselhaus, G. *Adv. Phys.* **1981**, *30*, 139. (b) Zabel, H.; Chow, P. C.; *Comments Solid State Phys.* **1986**, *12*, 225. (c) Ebert, L. B. *Annu. Rev. Mater. Sci.* **1976**, *6*, 181.
(6) DiSalvo, F. J.; Wilson, J. A.; Bagley, B. G.; Waszczak, J. V. *Phys. Rev. B* **1975**, *12*, 2220.

0001-4842/91/0124-0170$02.50/0 